Photothermal Readout of Surface-Arrayed Proteins: Attomole Detection Levels with Gold Nanoparticle Visualization

Matthias Koebel[†] and Matthew B. Zimmt*

Department of Chemistry, Brown University, Providence, Rhode Island 02912

Received: April 1, 2005; In Final Form: July 6, 2005

Transverse photothermal beam deflection (tPBD) is used to detect and quantify proteins arrayed on slides. The slides are "read" using an argon-ion excitation source. Optical absorption cross-sections of most proteins are too small for submonolayer coverages to produce thermal gradients of sufficient magnitude for detection using tPBD. Thus, surface-arrayed proteins are stained using mercaptoalkanoic acid coated gold nanoparticles (maa-AuNP). The large optical cross-sections of AuNP combined with electrolyte-induced AuNP aggregation afford a highly sensitive method for protein detection. Following maa-AuNP staining, the tPBD signal varies linearly with the amount of protein (Neutravidin) spotted on the slide surface: from 0.001 to 1.0 monolayer of protein. In a single 0.7 mm diameter array spot, the tPBD detection limit is 33 amol of Neutravidin or fewer than 55 protein molecules per μm^2. Despite the nonspecific nature of interactions between maa-AuNP and proteins, significant variations in protein staining efficacy are observed. The factors controlling staining are not elucidated in detail, but there is a correlation between protein pI and protein staining. Proteins with pI $\approx$ 6 are more effectively visualized by maa-AuNp than are more acidic or more basic proteins. The influence of AuNP diameter and mercaptoalkanoic acid chain length on protein staining and selectivity is investigated. The results demonstrate that AuNP staining coupled with tPBD detection constitutes a sensitive and practical method for probing protein arrays.

I. Introduction

Microarrays find use in medicine, biology, chemistry, and material science.[1] Nucleic acid microarrays are used in sequencing, polymorphism identification, pathogen characterization, and monitoring of nucleic acid (RNA) levels.[2] Protein and small molecule microarrays find application in proteomics and drug discovery.[3] Fluorescence is the primary method of detecting target binding on arrays, but alternate detection strategies are available. These include chemiluminescence,[4] colorimetric methods,[5] electrochemical methods,[6] Raman,[7] surface plasmon resonance (SPR) methods,[8] resonant light scattering[9] (RLS), and thermography.[10]

Colorimetric methods detect extinction of incident light; thus their dynamic range is frequently smaller than "zero background techniques" such as fluorescence and resonance light scattering. Colorimetric methods achieve high sensitivity target detection by exploiting the large plasmon resonance optical cross-sections of metal particles.[11] Metal particle "labels" also enhance detection sensitivities of other optical methods such as SPR, RLS, and thermography.[8−10] In this manuscript, we report application of the transverse photothermal beam deflection (tPBD) method to detect and quantify proteins arrayed on slides and visualized (stained) by physisorption of mercaptoalkanoic acid coated gold nanoparticles (maa-AuNP). The intensity of the tPBD signal from maa-AuNP visualized proteins varies linearly from 0.001 to 1.0 monolayer of adsorbed protein and has a detection limit below 50 amol in a 680 μm spot (<50 protein molecules/μm^2).

Photoacoustic and related all-optical methods detect small sample absorbance through the heat released following optical excitation.[12] The photothermal interference contrast (PIC) technique is one of the most sensitive photothermal methods, capable of detecting individual metal nanoparticles within polymers or bound to cell membranes.[13] Heat generated by optical excitation of a metal nanoparticle alters the optical path length in one arm of a PIC interferometer. IR thermography has been used to monitor catalytic activity in combinatorial libraries.[14] IR thermography combined with optical irradiation has been used to detect metal nanoparticle-labeled nucleic acids immobilized at surfaces.[10] The tPBD method employed in this report detects light absorption at interfaces. Heat generated by light absorption produces temperature and refractive index gradients in the media adjacent to the interface. These gradients alter the trajectory of a probe beam passing parallel to the interface. Because the gradients arise from a discontinuity in absorption (optical density) at the interface, the tPBD method is pseudo-confocal in nature. In-situ experiments can be performed in which one medium has significant absorbance at the pump beam wavelength. The tPBD method[15] detects optical densities as small as 10^{-6}. Although tPBD is less sensitive than PIC, the geometry of the tPBD experiment allows in-situ measurements, where an array slide is immersed in solution containing an absorbing stain.

Metal colloids are used frequently as histochemical stains for microscopy.[16] Metal particles conjugated to antibodies localize at specific tissue or cell sites. Specificity in metal nanoparticle localization can also be attained by conjugating small proteins, nucleic acids, carbohydrates, biotin, or other small molecules to the nanoparticle surface. Such surface modified nanoparticles are used in colorimetric and aggregation assays.[17] Electrostatic forces attract DNA[18] and proteins[19] to the surface of charged metal nanoparticles in a nonspecific manner.[20] In this initial application of the tPBD method for detection and quantification

* Corresponding author. E-mail: matthew_zimmt@brown.edu.
[†] Current address: College of Chemistry, University of California Berkeley, Berkeley, CA 94720.

10.1021/jp051671s CCC: $30.25
Published on Web 08/13/2005

of protein arrays, selective staining of specific proteins by metal nanoparticles was not desired. Thus, charged maa-AuNP were used to stain the arrayed proteins. The influence of alkyl chain length and nanoparticle size on detection sensitivity and selectivity was investigated.

II. Experimental Section

A. maa-AuNP Preparation. Small mercaptoalkanoic acid stabilized AuNPs were prepared using Kunitake's method.[21] A solution of tetrachloroauric acid ($HAuCl_4$, 48 mg, 1.05×10^{-4} mol) dissolved in 20 mL of doubly distilled water was added to 200 mL of boiling, doubly distilled water in a 500 mL flask. Once boiling restarted, a solution of trisodium citrate dihydrate (400 mg, 1.36×10^{-4} mol) and 3-mercaptopropanoic acid or 11-mercaptopropanoic acid (3.7×10^{-5} mol) in 20 mL of doubly distilled water was added. The mixture was refluxed and stirred until the color of the solution stopped changing: from yellow to red. Statistical analyses (Scion Image for Windows) of TEM images indicate mean particle diameters of 9.5 ± 2 nm.

Larger maa-AuNP particles were prepared in two steps. Citrate stabilized particles were synthesized using the Turkevitch method.[22] $HAuCl_4$ (48 mg, 1.1×10^{-4} mol) was added to 100 mL of double distilled water in a 500 mL round-bottom flask. The pH of the yellow solution was adjusted to 6.5 by addition of aqueous 1 M Na_2CO_3. The solution was boiled, and 10 mL of 1% trisodium citrate solution was added. The solution immediately darkened. After the mixture was refluxed for 1 h, the heat source was removed and sodium mercaptoalkanoate (5×10^{-5} mol) was added and stirred for 1 h. Statistical analyses (Scion Image for Windows) of TEM images indicate mean particle diameters of 17 ± 6 nm. The maa-AuNP-17 particles prepared using the Turkevitch method showed greater variability in electrolyte-induced aggregation characteristics (vide infra) than did the smaller maa-AuNP-9 particles. The Turkevitch particles with the greatest resistance to aggregation (i.e., those that tolerated the highest electrolyte concentrations) were formed when the solution temperature remained above 90 °C during the hour-long ligand exchange with sodium mercaptoalkanoate.

maa-AuNPs were precipitated by the addition of 1.6 M HCl (20 mL). The solid was isolated by centrifugation at 3000 rpm for 10 min. Following removal of the clear supernatant, the solid residue was washed with 20 mL of 0.05 M HCl and isolated by centrifugation. After three washes, the solid was suspended in 5 mL of doubly distilled water, and 50−100 μL of 0.25 M NaOH was added with stirring. The solid dissolved, and the solution turned a deep red color.

B. Array Preparation and Visualization. Proteins dissolved in 1:1 glycerol−100 mM phosphate buffered saline solution (PBS: 100 mM phosphate, 150 mM NaCl, pH 7.5) were spotted on aldehyde slides (ALS-25, CEL Associates) using a V & P Scientific (San Diego, CA) manual, 8-pin spotter. The volume delivered by each pin was determined by recording top and side views of the glycerol/PBS drop using a microscope objective and CCD camera. The typical diameter, height, and contact angle of the 1:1 glycerol/PBS drop were 680 μm, 90 μm, and 30°. The volume of a spherical section is $\pi \times h \times (h^2 + 0.75 \times d^2)/6$, where h and d are the drop height and diameter, respectively. The drop height may also be calculated as $d \times (1 + \cos\alpha)/(2 \times \sin\alpha)$, where α is the drop contact angle. Using the measured or calculated heights, the average drop volumes are 17 ± 3 nL. A volume of 20 nL was used to estimate the moles of protein applied.

After 1.5 h, spotted slides were inverted and placed onto the blocking buffer (3% Tween20 (Sigma), 5% sucrose, 0.2% NaN_3 in 100 mM PBS, pH 7.5).[23] After 1 min, the slides were removed, washed with blocking buffer, and placed on fresh blocking buffer for 5 min. After an additional wash with blocking buffer, each slide was washed with dilute phosphate buffered saline−Tween20 solution (PBST: 10 mM phosphate, 15 mM NaCl, 0.01% Tween20, pH 7.5), then immersed in PBST for 5 min, followed by a second wash with PBST. Slides were stained using a solution containing 50−200 nM maa-AuNP-9 or 1−5 nM maa-AuNP-17 in 40−90 mM MES (morpholinoethanesulfonic acid, 1 wt % Tween 20, pH 6.5) and gently agitated (electrical shaker, 70 rpm) for 30−60 min. After being stained, slides were washed with distilled water and dried using nitrogen (for storage) or immediately immersed in the water-filled tPBD cell. The proteins employed in this investigation were Neutravidin (Pierce, 31000), alkaline phosphatase (gift from Professor C. Seto), avidin (Sigma, A9275), bovine serum albumin (Sigma, A3902), pig liver esterase (Sigma, E3019), lysozyme (Sigma, L7651), and trypsin (Sigma, T4665).

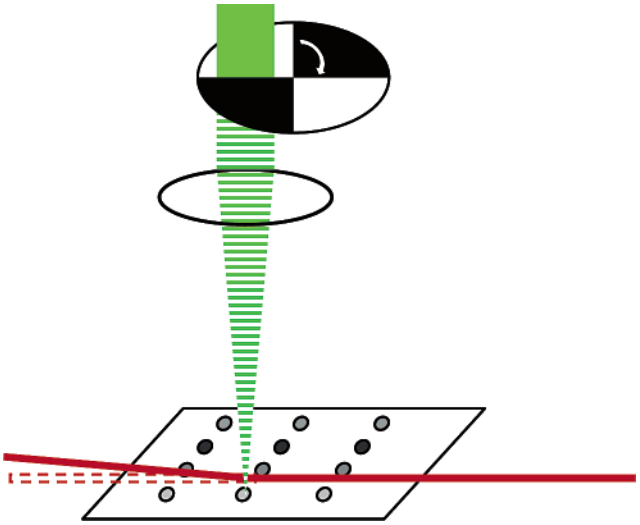

Figure 1. The tPBD experiment applied to maa-AuNP visualized microarrays. Absorption of modulated laser light (green) focused on the surface generates refractive index gradients that deflect the probe beam (red, entry from right). The deflection amplitude is measured in synchrony with the modulation frequency.

C. tPBD Measurements. Photothermal beam deflection methods (e.g., tPBD, mirage spectroscopy) are useful for measuring small optical absorbances.[24] tPBD can be used to measure spatial variation of absorbance at surfaces and in thin films.[25] In this application of tPBD, a mechanically chopped, continuous wave (CW) argon-ion "pump" laser beam (Coherent Innova 90; 488/514 nm lines) is focused to a 40 μm spot at the microarray slide surface (Figure 1). A CW He−Ne "probe" laser beam (Melles Griot, 633 nm, 10 mW) is directed parallel to the slide surface and focused to a 50 μm diameter where it crosses the pump beam. The tPBD cell containing the slide immersed in water is raised until it is adjacent to, and minimally clips, the probe beam. Photothermal deflection of the probe is detected using a split photodiode (UDT SPOT 2D, 135 μm gap). The outputs of the photodiode sectors are amplified differentially and recorded using a lock-in amplifier (Stanford Research SR510) synchronized to the pump beam chopping frequency (18 Hz for tPBD experiments in water). One-dimensional and two-dimensional tPBD images of microarrays are obtained by recording the lock-in signal while translating the slide relative to the crossed pump and probe laser beams.

D. Absorption Measurements. UV−visible spectra were recorded in a 96-well plate on a Tecan Safire plate reader

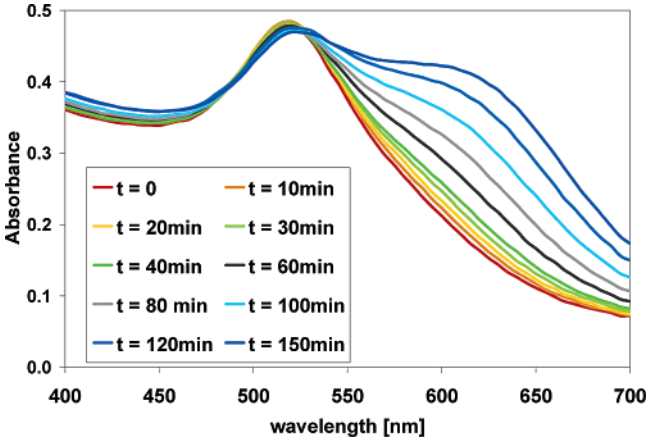

Figure 2. Absorption spectra of mpa-AuNP-17 in 46 mM MES (pH 6.5) as a function of time after electrolyte addition.

operated in absorbance mode. Equal volumes (10 μL) of maa-AuNP solutions were diluted into a constant volume (250 μL) of pH 6.35 MES buffer solution. MES concentrations ranged from 0 to 230 mM. The maa-AuNP stock solution concentration was adjusted to produce an absorbance reading of 0.4 at 520 nm after dilution in the buffer. Absorption spectra for each well were recorded from 400 to 700 nm with 5 nm resolution. Data collection for all wells was complete in 10 min and was repeated 15 times (150 min).

III. Results

A. Controlling maa-AuNP Aggregation. Slides spotted with Neutravidin (1000 μg/mL) were stained using 9 nm AuNP surface modified with mercaptopropanoic acid (mpa-AuNP-9). The intensities of the protein spots increased with increasing electrolyte concentration (MES or NaCl) in the buffer used during staining. Charged nanoparticles in aqueous solution remain dispersed at low ionic strengths but aggregate rapidly at high ionic strengths.[26] Electrolyte-induced aggregation broadens and red-shifts the absorption spectra of both the 9 and the 17 nm mpa-coated AuNP (Figure 2). The initially red solutions turn purple at rates that depend on the electrolyte concentration. Elevated electrolyte concentrations induce similar spectral changes in 17 nm AuNP surface modified with mercaptoundecanoic acid (mua-AuNP-17) but have no effect on the absorption spectrum of the smaller, 9 nm AuNP coated with mua (mua-AuNP-9). At sufficiently high electrolyte concentrations, colored solids precipitate from all four maa-AuNP solutions. The precipitates from the purple solutions (mpa-AuNP-9, mpa-AuNP-17, mua-AuNP-17) are deep blue, but the precipitate from mua-AuNP-9 solutions is the same red color as the unaggregated particles. The observation of a red precipitate unambiguously demonstrates aggregation of mua-AuNP-9 at high electrolyte concentration. The absence of a spectral shift precludes monitoring aggregation of mua-AuNP-9 by UV−vis spectroscopy.

Precipitation of maa-AuNP solids during visualization of protein arrays produces random tPBD signals in unspotted regions no matter how extensively the slides are rinsed. This degrades the experiment's sensitivity. On the other hand, visualization of protein slides with maa-AuNP under conditions where nanoparticles do not aggregate, that is, in low ionic strength buffer, generates small tPBD signals, which also reduces detection sensitivity. Optimal tPBD signals are obtained when the maa-AuNP solution changes from red to purple during the 20−100 min visualization treatment of the protein array. The electrolyte concentrations that promote aggregation on this time scale differ for each maa-AuNP. These concentrations were determined by recording AuNP solution absorbance spectra as a function of time at different electrolyte concentrations.

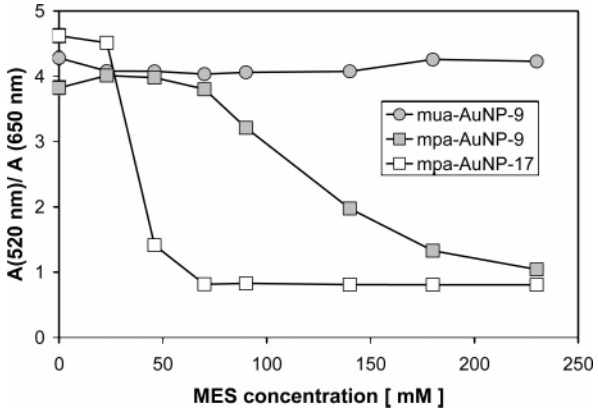

Figure 3. The absorbance ratio A(520 nm)/A(650 nm), a measure of aggregation, from spectra of mpa-AuNP-17, mpa-AuNP-9, and mua-AuNP-9 after 160 min in pH 6.4 solutions at different MES concentrations.

TABLE 1: Protein Properties

protein	MW (kDa)	pI
Neutravidin	66	6.3
BSA	66	4.3
trypsin	24	10−10.5
esterase	150	5.1−5.5
alkaline phosphatase	50	6.1
lysozyme	14	11
avidin	66	10.6

Figure 3 displays the ratio of absorbance at 520 nm, the peak wavelength of unaggregated maa-AuNP, to that at 650 nm (within the plasmon resonance absorption of aggregated maa-AuNP) after 160 min in solutions of different MES concentrations. At pH 6.4, MES concentrations greater than 40 mM induce extensive aggregation of the large, mpa-AuNP-17 colloid within 160 min. In 70 mM MES, the red to purple spectral evolution of mpa-AuNP-17 solutions is complete, and precipitate appears, within 40 min. Higher electrolyte concentrations are required to induce aggregation of the smaller maa-AuNP. The red to purple transition of mpa-AuNP-9 is less than 50% complete after 160 min in 90 mM MES. MES concentrations larger than 200 mM induced the complete spectral shift and precipitation within 2 h. The absorption spectrum of the small particles surface capped with the C-11 mercaptoundecanoic acid (mua-AuNP-9), did not exhibit a red-shift, even at MES concentrations higher than 200 mM. As noted above, this precludes a direct probe of this colloid's aggregation characteristics. maa-AuNP visualization of protein slides for tPBD measurements was performed using MES concentrations that, in 160 min, produced <50% of the red to purple color change for the specific maa-AuNP.

B. tPBD Detection of Surface Adsorbed Proteins Visualized with maa-AuNP. Electrostatic and hydrophobic interactions between maa-AuNP and proteins promote binding and staining of the array spots. These interactions should occur for all proteins but may not produce identical staining intensity. The variation in maa-AuNP staining of different proteins was investigated using AuNP of different sizes and capped with mpa or mua. The proteins used are listed in Table 1 along with some general properties. Figure 4 displays 1-D tPBD scans of arrays spotted with 1000 μg/mL protein solutions and stained using mpa-AuNP-9 in 46 mM MES buffer for 1 h. Significant variation in protein staining was observed. The tPBD signals

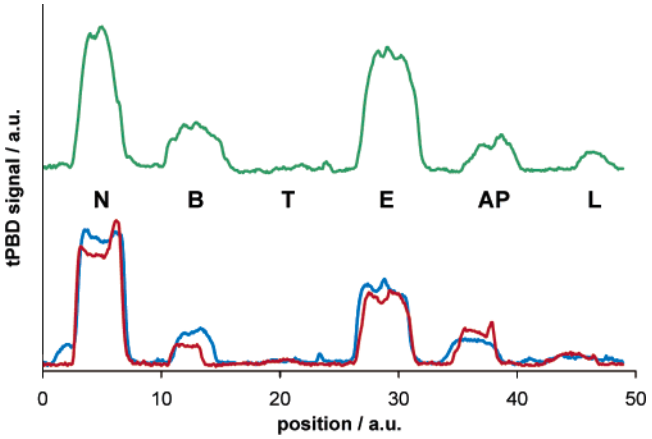

Figure 4. 1-D tPBD scans of six proteins visualized using mpa-AuNP-9 in 46 mM MES. From left to right, the proteins are Neutravidin, BSA, trypsin, esterase, alkaline phosphatase, and lysozyme. The red and blue lines are scans of two independently prepared slides (1000 μg/mL protein, except for AP: 400 μg/mL). The green line is a slide prepared using protein solution concentrations of 100 μg/mL. The average spot diameter is 670 μm.

from Neutravidin (N) and esterase (E) were 2−3 times as intense as the signals from bovine serum albumin (B) or alkaline phosphatase (AP). The signal from lysozyme (L) was 10−20% as large as the signal from Neutravidin. Trypsin (T) generated negligible tPBD signal (less than 5% of the Neutravidin signal intensity) when visualized with mpa-AuNP-9.

Factors that may contribute to the variation of tPBD signal intensities for different proteins include (1) the amount of protein bonded per spot at the array surface, (2) distributions in protein adsorption orientation or denaturation, (3) protein−maa-AuNP interactions that facilitate staining for adsorbed protein orientations, and (4) interference of maa-AuNP aggregation resulting from protein−maa-AuNP interactions. The amount of protein per array spot was varied to evaluate whether different extents of protein binding caused the variation in signal intensity from the six proteins. The moles of protein deposited per spot at 1000 μg/mL (~20 ng in a 20 nL volume) is more than a 20-fold excess over the amount needed to form a monolayer in a 0.7 mm diameter spot. Slides were also spotted using a 10-fold lower concentration (100 μg/mL), which is still sufficient protein to form a monolayer. If the proteins adhere to the slide with different propensities, a 10-fold reduction in the solution concentration should change the relative tPBD signal intensities unless both the 100 and the 1000 μg/mL spotting solutions produce a complete monolayer. The 1-D tPBD scans obtained following the standard protocol (binding, blocking, washing, and mpa-AuNP-9 development) exhibit similar relative signal intensities for the six proteins spotted at either 1000 or 100 μg/mL (Figure 4). Loading studies demonstrate that Neutravidin forms a complete monolayer when spotted at 1000 μg/mL (vide infra, Figures 5 and 7). Furthermore, staining with mpa-AuNP-17 (vide infra, Table 2) confirms that trypsin and lysozyme are present on the slides. These results indicate that protein adsorption to the slide is not the primary factor determining relative strengths of tPBD signals.

AuNP diameter and surface treatment influence the tPBD signal observed for the different proteins. Arrays spotted with 1000 μg/mL solutions were visualized using mpa-AuNP-17 or mua-AuNP-17 at 25 mM MES. Table 2 lists relative signal intensities for the proteins. With mpa-AuNP-17, Neutravidin and esterase generate the strongest tPBD signals. The signal from BSA is 30% as large as the Neutravidin signal.[27] In contrast with the relative intensities obtained with mpa-AuNP-9, the

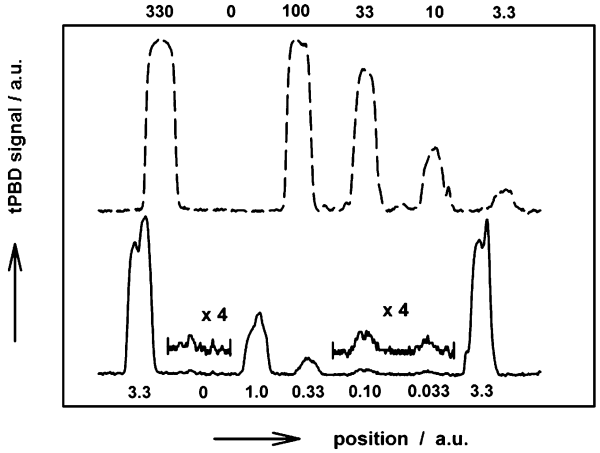

Figure 5. 1-D tPBD scans of slides spotted with Neutravidin and visualized with mpa-AuNP-9. The femtomoles of Neutravidin applied are listed adjacent to each spot. A 1000 μg/mL solution was used to prepare the 330 fmol spot. The upper 1-D scan employed 10 mW pump power. The lower 1-D scan employed 45 mW pump power. A ×4 expansion of the tPBD traces at the three lowest loadings is displayed above the lower plot.

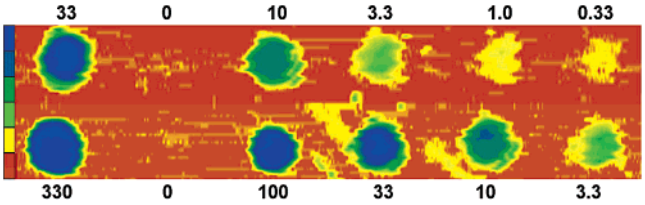

Figure 6. A false color, 2-D scan of a Neutravidin slide probed with mpa-AuNP-9. The femtomoles of Neutravidin applied are indicated adjacent to each spot. The colors signify the logarithm of the tPBD signal at each point (scale at left of figure: red = 0, yellow = 0.1, light green = 0.4, dark green = 1.2, dark blue = 2.4, light blue = 5).

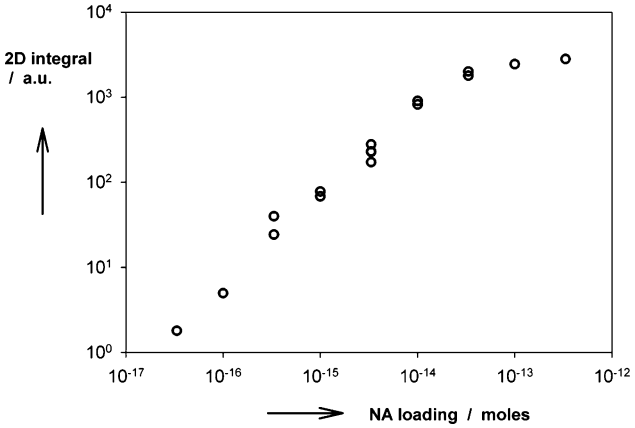

Figure 7. Log−log plot of integrated (signal intensity − background intensity) per spot for the 2-D scans versus moles of Neutravidin spotted.

signal for lysozyme stained with mpa-AuNP-17 is comparable to that of BSA and the signal from trypsin is readily detectable, about half as strong as BSA. Avidin (not visualized with mpa-AuNP-9) gives signals that are 60% as intense as Neutravidin. Overall, staining the proteins with the larger mpa-surface treated particles (mpa-AuNP-17) generates less signal intensity variation than staining with the smaller mpa-AuNP-9 particles.

1000 μg/mL protein arrays visualized with mua-AuNP-17 exhibit similar signal intensities for Neutravidin, esterase, and avidin. The signals for BSA, trpysin, and lysozyme are either very small or undetectable. Visualization with mua-AuNP-17 yields either strong or negligible signals ("all or nothing"

TABLE 2: Relative[a] tPBD Signal Intensities[b] for Proteins Visualized Using maa-AuNP

	protein						
maa-AuNP	Neutravidin	BSA	trypsin	esterase	alkaline phosphatase	avidin	lysozyme
mpa-AuNP-9	1.0	0.3	0.0	0.8	0.3	−[c]	0.1
mpa-AuNP-17	1.0	0.3	0.2	0.9	−[c]	0.6	0.4
mua-AuNP-17	1.0	0.1	0.0	0.8	−[c]	0.6	0.1

[a] Neutravidin signal used as the reference. Standard deviations of the relative intensities are ±0.1. [b] Integrated intensities for the entire spot (see Results, section C). [c] Not measured.

response) for the six proteins studied. The same, large nanoparticles coated with mpa (mpa-AuNP-17) generate more subtle signal intensity variations among the different proteins.[28]

C. tPBD Detection Limits: Neutravidin Visualized with mpa-AuNP-9. Neutravidin was used to evaluate the dependence of tPBD signal on protein surface loading because this protein gives the largest signals. Neutravidin was spotted on aldehyde slides using 0.1−1000 μg/mL solutions in 1:1 glycerol:PBS (see Experimental Section). For these spotting concentrations, the amount of protein applied per spot ranged from 33 attomole (amol) to 330 femtomole (fmol). One-dimensional tPBD scans of slides spotted with 33 amol to 330 fmol of Neutravidin are displayed in Figure 5. A blank was spotted in each row (second position from the left) using the glycerol/PBS solution containing no Neutravidin. The blank establishes the background signal associated with spotting, and the data in regions between the spots characterize the background and noise. The two rows were interrogated using 10 mW pump power (3.3−330 fmol/spot) or 45 mW pump power (0.033−3.3 fmol/spot). tPBD signal intensity scales linearly with pump power;[15] thus the two data sets were analyzed jointly following normalization for pump power and lock-in amplifier settings. When scaled in this manner, the signal intensities from the 3.3 fmol spots in the two scans agree to within 20%. The scanned spot edges are sharp, exhibiting a 10−90% rise across a distance of 80 μm. The intensities of the 33, 100, and 330 fmol spots are similar (top row), indicating saturation of Neutravidin adsorbed per spot for loadings greater than 33 fmol (vide infra) or saturation of the visualization afforded by mpa-AuNP-9. The tPBD signal for 0.033 fmol (33 amol) of Neutravidin is twice as large as the blank and exhibits a signal-to-noise ratio of ∼4:1. This spot loading is the detection limit for the current experimental setup. Provided all Neutravidin applied in the spot binds to the slide, the detection limit is 55 Neutravidin molecules per μm^2 or 120 zmol in a 40 μm diameter spot. Greater detection sensitivity may be attained using higher pump laser power, by amplifying the AuNP absorption, for example, with silver,[5e] or by using photothermal interference methods.[13]

A false-color two-dimensional scan of Neutravidin slide prepared with spot loadings between 0.33 and 330 fmol was obtained by combining 1-D scans collected at 25 μm intervals (Figure 6). The color scale reflects the logarithm of signal intensity. The yellow streaks to the left of the 33 and 10 fmol spots (lower row) indicate some spot smearing. The tPBD signal intensity in excess of background (0 fmol spots) was integrated over the 2-D image of each feature. A log−log plot of the integrated signal versus the moles of protein spotted is linear, with a slope of 1, between 33 amol and 33 fmol of Neutravidin (Figure 7). The tPBD signal saturates for larger amounts of applied protein. The Neutravidin tetramer diameter is approximately 5 nm.[29] A densely packed monolayer (for a flat surface and no protein denaturation) would contain ∼24 fmol in a 680 μm diameter spot. Saturation of the tPBD signal for protein loadings comparable to this value (33 fmol) suggests that protein monolayer formation, not saturation of maa-AuNP visualization, is responsible for the saturation of tPBD signal intensity at the highest spot loadings.

IV. Discussion

A. Aggregation. Electrolyte-induced aggregation of charged nanoparticles is a well-known phenomenon. The different maa-AuNP samples exhibit different dependences of aggregation rate on electrolyte concentration. MES concentrations above 100 mM are needed to induce rapid aggregation of the small, mpa-coated nanoparticles (mpa-AuNP-9). The larger nanoparticles, mpa-AuNP-17, aggregate rapidly at lower concentrations, <40 mM MES. Controlled formation of maa-AuNP layers at surfaces has been demonstrated using Cu^{2+} and Zn^{2+} ions.[30] Sub-millimolar concentrations of divalent metal ions induce aggregation of maa-AuNP.[31] Selective aggregation of AuNP may also be induced with properly tailored metal chelating ligands at the nanoparticle surface.[32] These approaches could be used to increase the tPBD signal amplitude and reduce background noise by controlling the growth of AuNP structures at the surface under conditions where solution aggregation of AuNP does not occur.

B. Protein Detection and Identification. Protein staining by maa-AuNP is somewhat selective. Three of the seven proteins, Neutravidin, esterase, and avidin, are effectively visualized by all three maa-AuNP. The relative staining propensities of these three proteins are nearly unchanged for the different AuNP sizes and surface coatings. Trypsin and lysozyme are poorly visualized by two of the maa-AuNP. Only mpa-AuNP-17 staining generates useful tPBD signals for these two proteins. mpa-AuNP-17 visualizes all of the proteins but still exhibits 5−6-fold intensity differences. Switching to the mercaptoundecanoic acid coating on AuNP-17 affords almost no tPBD signal for BSA, trypsin, and lysozyme.

Hydrophobic and electrostatic forces are involved in binding of AuNP to proteins.[20] Protein charge, surface composition, and deformability all may play a role in determining AuNP staining. The specific interactions responsible for protein staining by the AuNP were not elucidated in these experiments. Furthermore, the extent to which maa-AuNP binding detects or induces[19,20] denatured protein structures in the microarray[33] was not evaluated. Relative staining proficiency of the proteins (relative to Neutravidin) does not correlate with protein molecular weight but does exhibit a rough correlation with protein pI (Figure 8). The fact that low pI proteins stain less effectively than Neutravidin might arise from electrostatic repulsion between the net negatively charged proteins and maa-AuNP under the visualization conditions (pH 6.4). A corollary, that high pI proteins are stained better than Neutravidin by the negative maa-AuNP at pH 6.4, is contradicted by the data. It appears that structural factors other than the bound charges on the protein and maa-AuNP charges determine the staining efficacy.

The alkyl chains on the surface of the AuNP interact with proteins and can influence protein structure[19] and function.[20]

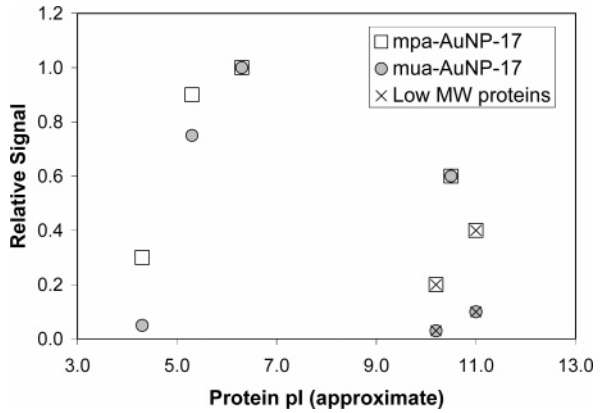

Figure 8. Relative tPBD signal intensities of protein arrays (1000 μg/mL) visualized with mpa-AuNP-17 and mua-AuNP-17 particles in pH 6.4, 25 mM MES buffer. The signal intensities are normalized relative to the signal from Neutravidin stained by the corresponding maa-AuNP.

The mua-coated particles have greater alkyl content than the mpa-AuNP and, thus, might interact more strongly with larger proteins or with proteins whose hydrophobic regions are more accessible. We do not have absolute measures of protein staining by the different maa-AuNP. However, the relative ratios (relative to the Neutravidin signal) suggest that proteins other than the avidins are stained less effectively by the more hydrophobic mua-AuNP-17 than by the less hydrophobic mpa-AuNP-17.[34] At this point, we lack data to discriminate among potential explanations, for example, less mobile alkyl chains or less water content in the alkyl chains of mua-AuNP. Interestingly, mpa-AuNP-17 and mua-AuNP-17 stain avidin equally effectively (relative to Neutravidin staining). Neutravidin is prepared by removing cationic carbohydrates from the surface of avidin. Removing the positively charged carbohydrates (avidin → Neutravidin) increases staining efficacy by mpa-AuNP and mua-AuNP to a similar extent.

In principle, the dissimilar staining efficacies of proteins by different maa-AuNP preparations could be used to detect and identify proteins in an "electronic nose" approach.[35] To this end, we prepared 11-trimethylammonium undecanethiol coated AuNP to probe whether visualization with a cationic AuNP gives significantly different or distinctive protein staining. While this "cationic AuNP" visualized the proteins, the background staining of the slides was too great for quantitative studies.

C. tPBD Sensitivity. The minimum absorbance detectable in a tPBD measurement depends on the pump laser power. For experiments performed in air, the product of the surface absorbance and the pump laser power must be $0.1-1.0 \times 10^{-5}$ W or larger.[15,36] If one maa-AuNP binds per protein, the absorbance from staining 10 fmol of protein in a 680 μm diameter spot is 0.15 at the peak wavelength 520 nm.[37] The product of the sample absorbance and the maximum pump power used in these experiments (45 mW) is 7×10^{-3} W, which is 2 orders of magnitude larger than the detection limit. For 33 amol of maa-AuNP, the product of the sample absorbance and pump power is 2×10^{-5} W, close to the published detection limit of the tPBD method in air. Two features of the experiment as implemented here enhance the sensitivity. The tPBD signal from a sample measured in water is at least 50 times larger than that for the same sample measured in air.[38] Second, aggregation of the maa-AuNP attracts more than one maa-AuNP per protein. Spot coloration increases with longer exposures to the maa-AuNP solution. Presumably, additional maa-AuNP aggregates adhere to the layer of maa-AuNP stuck directly to the proteins.[39] The relative tPBD intensities of different proteins or of a single protein spotted at different loadings remain relatively constant for visualization times between 20 and 90 min. Thus, any maa-AuNP multilayers that may form during this staining period grow at rates that reflect the initial maa-AuNP staining probability. Slides visualized overnight have larger extinction but smaller variation of signal intensity with amount or identity of protein loaded. When staining is performed for long time intervals, spots must eventually darken at rates that do not reflect the identity of the protein in the spot.

As noted above, the detection limit achieved with Neutravidin corresponds to 55 proteins per μm^2. This is comparable to the detection limit afforded by Cy-3 fluorescence sensing[40] of target capture (10^5 strands) in high-density DNA microarrays containing 10^7 or more DNA probes per 50 μm feature.[41] The detection limit of the tPBD experiment can be lowered by using higher laser powers because AuNPs are not prone to photobleaching. Sensitivity might also be increased through AuNP catalysis of silver reduction.[5e,40] Detection using photothermal interference methods[13] should significantly enhance sensitivity but would exclude in-situ studies in which AuNP stains are present in the fluid.

V. Conclusion

The transverse photothermal beam deflection (tPBD) technique affords sensitive detection of surface absorbance with sub-100 μm spatial resolution. This method can be used to readout microarrays, provided array spots can be visualized. Fluorescence is the principal method used to tag and evaluate arrays. Highly fluorescent molecules release little energy as heat and often are prone to photobleaching, making them unsuitable as stains for photothermal methods. Colorimetric detection methods frequently employ intensely colored metal nanoparticles. Metal nanoparticles are ideal photothermal stains as they are nonluminescent, resistant to photodegradation, and their surfaces can be functionalized to provide specific or nonspecific adherence to target structures. Combining the high sensitivity of tPBD methods (absorbances smaller than 10^{-5}) with target visualization using the large cross-sections of metal nanoparticles provides a convenient and sensitive technique to readout protein and other microarrays.

In this investigation, surface-arrayed proteins were visualized using mercaptoalkanoic acid coated gold nanoparticles (maa-AuNP). Despite the absence of protein cofactors, inhibitors, or other protein specific ligands in the AuNP coating, maa-AuNP staining of proteins exhibits moderate selectivity. Proteins that are neutral (pI $\approx$ 6) under the conditions used for AuNP visualization (pH 6.4) are stained more intensely than more acidic (pI 4) or more basic (pI 10) proteins. Because the tPBD signal varies with the identity of the surface-arrayed protein, the staining selectivity must arise from direct interactions between the maa-AuNP and the protein. Slides visualized with maa-AuNP under conditions that control maa-AuNP aggregation (selected electrolyte concentrations and 30−90 min visualization times) maintain constant ratios of tPBD signal intensities for different proteins or different surface concentrations of a single protein, even as the absolute intensity of each spot increases. Visualization for extended times (overnight) increases protein spot intensities, produces smaller variation of signal intensities for different proteins or protein concentrations, and increases the tPBD signal in regions without protein. These treatments promote formation of maa-AuNP multilayers.

The tPBD signal varies linearly for 0.7 mm diameter spots prepared using 33 amol to 33 fmol of Neutravidin. The tPBD signal saturates for spots prepared with larger amounts of this

protein, consistent with the formation of a Neutravidin monolayer. The lower detection limit, 33 amol, corresponds to less than 0.001 monolayer of protein or fewer than 55 Neutravidin molecules per μm^2. This detection limit is sufficient for many protein (or DNA hybridization) studies and is comparable to practical detection sensitivities of commercial fluorescence scanners.[42] The linear dependence of tPBD signal on protein surface loading demonstrates that the technique can be used to quantify the amount of protein present on a slide.

There are innumerable surface modifications for AuNP. It should be possible to target selectively a specific protein using an AuNP surface modified with a ligand, inhibitor, or antigen. Subsequent development with a second AuNP that binds to the first AuNP or with an alternate stain, such as silver, could enhance selectivity in tPBD analyses. Related experiments are currently in progress.

Acknowledgment. Financial support from Brown University and the National Science Foundation (CHE-0108945) is acknowledged. We thank Professor John Oliver (Brown University, GeneSpectrum Inc.) for helpful discussions and use of the manual spotter, Professor Sun for recording TEM images of the maa-AuNP, Professors Seto and Cane for protein samples, Professor Basu for use of the Tecan plate reader, and Professor Weber for use of the Ar-ion laser.

Supporting Information Available: Two TEM images of mpa-AuNP-9 and two TEM images of mua-AuNP-17. This material is available free of charge via the Internet at http://pubs.acs.org.

References and Notes

(1) (a) Weeraratna, A. T.; Nagel, J. E.; De Mello-Coelho, V.; Taub, D. D. *J. Clin. Immunol.* **2004**, *24*, 213. (b) Xiang, X.-D.; Sun, X.; Briceno, G.; Lou, Y.; Wang, K.-A.; Chang, H.; Wallace-Freedman, W. G.; Chen, S.-W.; Schultz, P. G. *Science* **1995**, *268*, 1738. (c) Stears, R. L.; Martinsky, T.; Schena, M. *Nat. Med.* **2003**, *9*, 140.

(2) (a) Chee, M.; Yang, R.; Hubbell, E.; Berno, A.; Huang, X. C.; Stern, D.; Winkler, J.; Lockhart, D. J.; Morris, M. S.; Fodor, S. P. A. *Science* **1996**, *274*, 610. (b) McCormick, M. *PharmaGenomics* **2004**, 60. (c) Call, D. R.; Borucki, M. K.; Loge, F. J. *J. Microbiol. Methods* **2003**, *53*, 235.

(3) (a) MacBeath, G.; Koehler, A. N.; Schreiber, S. L. *J. Am. Chem. Soc.* **1999**, *121*, 7967. (b) Kusnezow, W.; Pulli, T.; Witt, O.; Hoheisel, J. D. *Protein Microarrays* **2005**, 247. (c) Salisbury, C. M.; Maly, D. J.; Ellman, J. A. *J. Am. Chem. Soc.* **2002**, *124*, 14868. (d) Zhu, Q.; Uttamchandani, M.; Li, D.; Lesaicherre, M. L.; Yao, S. Q. *Org. Lett.* **2003**, *5*, 1257. (e) Winssinger, N.; Harris, J. L.; Backes, B. J.; Schultz, P. G. *Angew. Chem., Int. Ed.* **2001**, *40*, 3152. (f) Zhu, H.; Bilgin, M.; Snyder, M. *Annu. Rev. Biochem.* **2003**, *72*, 783. (g) Espina, V.; Woodhouse, E. C.; Wulfkuhle, J.; Asmussen, H. D.; Petricoin, E. F.; Liotta, L. A. *J. Immunol. Methods* **2004**, *290*, 121. (h) Falsey, J. R.; Renil, M.; Park, S.; Li, S.; Lam, K. S. *Bioconjugate Chem.* **2001**, *12*, 346. (i) Kodakek, T. *Chem. Biol.* **2001**, *8*, 105.

(4) (a) Kricka, L. J. *Anal. Chim. Acta* **2003**, *500*, 279. (b) Huang, R.-P. *J. Immunol. Methods* **2001**, *255*, 1.

(5) (a) Liang, R.-Q.; Li, W.; Li, Y.; Tan, C.-y.; Li, J.-X.; Jin, Y.-Xi.; Ruan, K.-C. *Nucleic Acids Res.* **2005**, *33*, e17/1. (b) Nath, N.; Chilkoti, A. *Anal. Chem.* **2002**, *74*, 504. (c) Alexandre, I.; Hamels, S.; Dufour, S.; Collet, J.; Zammatteo, N.; De Longueville, F.; Gala, J.-L.; Remacle, J. *Anal. Biochem.* **2001**, *295*, 1. (d) Haes, A. J.; Stuart, D. A.; Nie, S.; Van Duyne, R. P. *J. Fluoresc.* **2004**, *14*, 355. (e) Taton, T. A.; Mirkin, C. A.; Letsinger, R. L. *Science* **2000**, *289*, 1757.

(6) (a) Dill, K.; Montgomery, D. D.; Ghindilis, A. L.; Schwarzkopf, K. R.; Ragsdale, S. R.; Oleinikov, A. V. *Biosens. Bioelectron.* **2004**, *20*, 736. (b) Turcu, F.; Schulte, A.; Hartwich, G.; Schuhmann, W. *Angew. Chem., Int. Ed.* **2004**, *43*, 3482. (c) Kojima, K.; Hiratsuka, A.; Suzuki, H.; Yano, K.; Ikebukuro, K.; Karube, I. *Anal. Chem.* **2003**, *75*, 1116.

(7) (a) Cao, Y. C.; Jin, R.; Nam, J.-M.; Thaxton, C. S.; Mirkin, C. A. *J. Am. Chem. Soc.* **2003**, *125*, 14676. (b) Allain, L. R.; Vo-Dinh, T. *Anal. Chim. Acta* **2002**, *469*, 149.

(8) (a) Kanda, V.; Kariuki, J. K.; Harrison, D. J.; McDermott, M. T. *Anal. Chem.* **2004**, *76*, 7257. (b) Goodrich, T. T.; Lee, H. J.; Corn, R. M. *Anal. Chem.* **2004**, *76*, 6173. (c) Otsuki, S.; Yamada, H.; Iwahashi, H.; Tamada, K. *Chem. Sens.* **2004**, *20 (Suppl. B)*, 514. (d) Wegner, G. J.; Wark, A. W.; Lee, H. J.; Codner, E.; Saeki, T.; Fang, S.; Corn, R. M. *Anal. Chem.* **2004**, *76*, 5677.

(9) (a) Bao, P.; Frutos, A. G.; Greef, C.; Lahiri, J.; Muller, U.; Peterson, T. C.; Warden, L.; Xie, X. *Anal. Chem.* **2002**, *74*, 1792. (b) Raschke, G.; Kowarik, S.; Franzl, T.; Klar, T. A.; Feldmann, J.; Nicthl, A.; Kürzinger, K. *Nano Lett.* **2003**, *3*, 935.

(10) (a) Lowe, L. B.; Brewer, S. H.; Kraemer, S.; Fuierer, R. R.; Qian, G.; Agbasi-Porter, C. O.; Moses, S.; Franzen, S.; Feldheim, D. L. *J. Am. Chem. Soc.* **2003**, *125*, 14258. (b) Franzen, S.; Feldheim, D. Methods for detection of nucleic acids using nanoparticle-coupled probes and IR thermography. U.S. Patent Appl. Publ. 2004; CAN 141:237722 AN 2004: 759718.

(11) (a) Link, S.; El-Sayed, M. A. *J. Phys. Chem. B* **1999**, *103*, 8410. (b) Link, S.; El-Sayed, M. A. *J. Phys. Chem. B* **1999**, *103*, 4212.

(12) (a) Barker, B. D.; Larsen, R. W. *J. Biochem.* **2001**, *5*, 407. (b) Braslavsky, S. E.; Heibel, G. E. *Chem. Rev.* **1992**, *92*, 1381. (c) Meyer, P. L.; Sigrist, M. W. *Rev. Sci. Instrum.* **1990**, *61*, 1779−807. (d) McDonald, F. A. *Can. J. Phys.* **1986**, *64*, 1023.

(13) (a) Boyer, D.; Tamarat, P.; Maali, A.; Lounis, B.; Orrit, M. *Science* **2002**, *297*, 1160. (b) Cognet, L.; Tardin, C.; Boyer, D.; Choquet, D.; Tamarat, P.; Lounis, B. *Proc. Natl. Acad. Sci. U.S.A.* **2003**, *100*, 11350. (c) Kimura, H.; Nagao, F.; Kitamura, A.; Sekiguchi, K.; Kitamori, T.; Sawada, T. *Anal. Biochem.* **2000**, *283*, 27. (d) Mawatari, K.; Kitamori, T.; Sawada, T. *Anal. Chem.* **1998**, *70*, 5037.

(14) Holzwarth, A.; Schmidt, H.-W.; Maier, W. F. *Angew. Chem., Int. Ed.* **1998**, *37*, 2644.

(15) Jackson, W. B.; Amer, N. M.; Boccara, A. C.; Fournier, D. *Appl. Opt.* **1981**, *20*, 1333.

(16) (a) Goodman, S. L.; Hodges, G. M.; Livingston, D. C. *Scanning Electron Microsc.* **1980**, *II*, 133. (b) Gu, J.; de Mey, J.; Moeremans, M.; Polak, J. M. *Regul. Pept.* **1981**, *1*, 365.

(17) (a) Boal, A. K.; Ilhan, F.; DeRouchey, J. E.; Thurn-Albrecht, T.; Russell, T. P.; Rotello, V. M. *Nature* **2000**, *404*, 746. (b) Storhoff, J. J.; Lazarides, A. A.; Mucic, R. C.; Mirkin, C. A.; Letsinger, R. L.; Schatz, G. C. *J. Am. Chem. Soc.* **2000**, *122*, 4640. (c) Liu, J.; Lu, Y. *J. Fluoresc.* **2004**, *14*, 343. (d) Aslan, K.; Luhrs, C. C.; Perez-Luna, V. H. *J. Phys. Chem. B* **2004**, *108*, 15631. (e) Hone, D. C.; Haines, A. H.; Russell, D. A. *Langmuir* **2003**, *19*, 7141.

(18) Li, H.; Rothberg, L. J. *J. Am. Chem. Soc.* **2004**, *126*, 10958.

(19) Jiang, X.; Jiang, J.; Jin, Y.; Wang, E.; Dong, S. *Biomacromolecules* **2005**, *6*, 46.

(20) (a) Hong, R.; Emrick, T.; Rotello, V. M. *J. Am. Chem. Soc.* **2004**, *126*, 13572. (b) Simard, J. M.; Szymanski, B.; Rotello, V. M. *Med. Chem.* **2005**, *1*, 153. (c) Fischer, N. O.; McIntosh, C. M.; Simard, J. M.; Rotello, V. M. *Proc. Natl. Acad. Sci. U.S.A.* **2002**, *99*, 5018. (d) Fischer, N. O.; Verma, A.; Goodman, C. M.; Simard, J. M.; Rotello, V. M. *J. Am. Chem. Soc.* **2003**, *125*, 13387. (e) Baldini, L.; Wilson, A. J.; Hong, J.; H., A. D. *J. Am. Chem. Soc.* **2004**, *126*, 5656. (f) Jain, R. K.; Hamilton, A. D. *Org. Lett.* **2000**, *2*, 1721.

(21) Kunitake, T.; Yonezawa, T. *Colloids Surf., A* **1999**, *149*, 193−199.

(22) Turkevitch, J.; Stevenson, P. C.; Hillier, J. *Discuss. Faraday Soc.* **1951**, *11*, 55−75.

(23) Li, Y.; Reichert, W. M. *Langmuir* **2003**, *19*, 1557.

(24) (a) Jackson, W. B.; Amer, N. M.; Boccara, A. C.; Fournier, D. *Appl. Opt.* **1981**, *20*, 1333. (b) Gheeraer, E.; Deneuville, A.; Bustarret, E.; Fontaine, F. *Diamond Relat. Mater.* **1995**, *4*, 684.

(25) (a) Tzolov, M.; Koch, V. P.; Bruetting, W.; Schwoerer, M. *Synth. Met.* **2000**, *109*, 85. (b) Cifre, J.; Roger, J. P. *Thin Solid Films* **1998**, *320*, 198.

(26) (a) *Colloidal Gold: Principles, Methods, and Applications*; Hayat, M. A., Ed.; Academic Press: San Diego, CA, 1991. (b) Warner, M. G.; Reed, Scott M.; Hutchison, J. E. *Chem. Mater.* **2000**, *12*, 3316. (c) Baschong, W.; Lucocq, J. M.; Roth, J. *Histochemistry* **1985**, *83*, 409. (d) Levy, R.; Thanh, N. T. K.; Doty, R. C.; Hussain, I.; Nichols, R. J.; Schiffrin, D. J.; Brust, M.; Fernig, D. G. *J. Am. Chem. Soc.* **2004**, *126*, 10076. (e) Shipway, A. N.; Lahav, M.; Gabai, R.; Willner, I. *Langmuir* **2000**, *16*, 8789.

(27) Alkaline phosphatase was not used after the study with mpa-AuNP-9 because of low solubility. Avidin was used in its place but is not discussed in this comparison.

(28) Experiments to determine which maa-AuNP gives the most intense stain were not performed.

(29) Pugliese, L.; Coda, A.; Malcovati, M.; Bolognesi, M. *J. Mol. Biol.* **1993**, *231*, 698−710.

(30) Zamborini, F. P.; Hicks, J. F.; Murray, R. W. *J. Am. Chem. Soc.* **2000**, *122*, 4514−15.

(31) (a) Kim, Y.; Johnson, R. C.; Hupp, J. T. *Nano Lett.* **2001**, *1*, 165. (b) Berchmans, S.; Thomas, P. J.; Rao, C. N. R. *J. Phys. Chem. B* **2002**, *106*, 4647.

(32) Norsten, T. B.; Frankamp, B. L.; Rotello, V. M. *Nano Lett.* **2002**, *2*, 1345.

(33) Eickoff, H.; Konthur, Z.; Lueking, A.; Lehrach, H.; Walter, G.; Nordhoff, E.; Nyarsik, L.; Buessow, K. *Adv. Biochem. Eng./Biotechnol.* **2002**, *77*, 103−112.

(34) Alternative explanations for the smaller mua-AuNP-17 staining of proteins in Figure 8 include (a) particularly effective staining of Neutravidin (relative to other proteins) by mua-AuNP-17 or (b) by particularly ineffective staining of Neutravidin (relative to other proteins) by mpa-AuNP-17.

(35) (a) Schauer, C. L.; Steemers, F. J.; Walt, D. R. *J. Am. Chem. Soc.* **2001**, *123*, 9443. (b) McCleskey, S. C.; Floriano, P. N.; Wiskur, S. L.; Anslyn, E. V.; McDevitt, J. T. *Tetrahedron* **2003**, *59*, 10089. (c) Rangin, M.; Basu, A. *J. Am. Chem. Soc.* **2004**, *126*, 5038.

(36) Wu, Z.; Tang, J.; Shi, B. *NIST Spec. Publ. 775* **1988**, 385−89.

(37) (a) The 520 nm extinction coefficient of a 9 nm AuNP without a thiol monolayer is $\sim 8 \times 10^7$ M^{-1} cm^{-1}.[37b] Based on studies of 1.9 and 5.6 nm decanethiolate coated AuNP,[37c] the estimated extinction coefficient of maa-AuNP-9 should be 6×10^7 M^{-1} cm^{-1}. The 0.15 optical density calculation assumes the extinction coefficient is 5×10^7 M^{-1} cm^{-1}. (b) Link, S.; El-Sayed, M. A. *J. Phys. Chem. B* **1999**, *103*, 8410−26. (c) Maye, M. M.; Han, L.; Kariuki, N. N.; Ly, N. K.; Chan, W.-B.; Luo, J.; Zhong, C.-J. *Anal. Chim. Acta* **2003**, *496*, 17.

(38) Bennett, J. M.; Pelletier, E.; Albrand, G.; Borgogno, J. P.; Lazarides, B.; Carniglia, C. K.; Schmell, R. A.; Allen, T. H.; Tuttle-Hart, T.; Guenther, K. H.; Saxer, A. *Appl. Opt.* **1989**, *28*, 3303−17.

(39) Preliminary AFM measurements indicate that the maa-AuNP spot produced by overnight staining of proteins is many layers thick.

(40) Alexandre, I.; Hamels, S.; Dofour, S.; Collet, J.; Zammatteo, N.; De Longueville, F.; Gala, J.-L.; Remacle, J. *Anal. Biochem.* **2001**, *295*, 1.

(41) Winzeler, E. A.; Richards, D. R.; Conway, A. R.; Goldstein, A. L.; Kalman, S.; McCullough, M. J.; McCusker, J. H.; Stevens, D. A.; Wodicka, L.; Lockhart, D. J.; Davis, R. W. *Science* **1998**, *281*, 1194.

(42) http://www.imstar.fr/products/cytology/osa/characteristics/.